Gain scheduling controller design for wind systems using a data driven algorithm

Adriana Burlibaşa, Marian Barbu, Emil Ceangă

Department of Automatic Control and Electrical Engineering
"Dunarea de Jos" University of Galati Domneasca 47, 800008, Galaţi, România
Marian.Barbu@ugal.ro

***Abstract*— The paper presents a data-based synthesis method for power control algorithm of a wind turbine in full-load operating region, within a general strategy of gain scheduling type. The proposed method is based on the existence of several efficient solutions for the generation of a detailed mathematical model for a high-power wind system that by its simulation in different operating regimes can provide the necessary data obtained for the design procedure. The synthesis of the control algorithm is based on the construction of a dynamic compensator which can quickly provide the parameters of a PI control law for the rotational speed loop. In the paper the effects of the drive train torsional vibrations in the controller synthesis are analyzed by numerical simulation. Some results obtained with the gain-scheduling control approach are also presented.**

Keywords—data-driven design; windmill; identification; PI control

I. INTRODUCTION

The automatic control of the wind energy conversion systems (WECS) represents an important research subject, due to its significant contributions in increasing the performances of these systems. In present, a large diversity of proposed WECS control solutions can be found in literature, for numerous particularities of the mathematical process model [1] - [5]. The modelling methodology of WECS emphasizes the aerodynamic subsystem, in which the tower-blade-mechanical transmission assembly is treated as a multi-resonant dynamic subsystem. This is excited by the wind speed component which contains the rotational turbulence [6].

Currently there is a very good experience in modelling the WECS in detail, including software tools to generate mathematical models [7] - [9]. Given the possibility of using detailed WECS mathematical models, a relatively simple solution to generate control laws is to adopt a data-based design procedure. Under this approach, the data are provided by simulating the detailed WECS model in different operating regimes, depending on the requirements of the design procedure. In this paper, a data-based design procedure is used for the control algorithm synthesis of a turbine rotational speed in the full-load region. It is known that an essential approach to controlling WECS is the gain scheduling control (GSC) [1], [3], [4]. The procedure proposed in the paper aimed at calculating the "local" controllers within the GSC. Compared to other methods from the literature, the proposed procedure allows direct obtaining of classical "local" PI controllers using a detailed model of WECS. The performances of the obtained gain scheduling controller are illustrated in a WECS with a rated power of 2 MW. The procedure for the data controller design is included into the WECS's control structure where the blade pitch control is performed within a control loop that keeps the rotational speed to the rated value, when the torque is maintained to the rated value.

The paper is structured as follows: Section II presents the system modelling and the WECS' control structure. Section III presents the data-based design procedure of the rotational speed controller. Section IV contains the numerical results obtained with the gain-scheduling control approach. The final section is dedicated to conclusions.

II. WIND SYSTEM MODELLING AND CONTROL

A. Wind system modelling

Since the mathematical modelling of wind systems is a well-known problem, only the basic components of the model will be mentioned below. The modular construction of the mathematical model has been adopted for us to be able to select the option of including or not some subsystems such as those for the damping of the tower oscillations and/or torsional oscillations.

The wind system was structured on two interacting subsystems: a) the aerodynamic subsystem, to which the flexible drive train was added, and b) the electromagnetic subsystem.

Figure 1 presents the structure of the first subsystem, on which the following notations are used: v_m - mean wind speed; v – relative air speed in relation to the blade, assuming that the tower and the blades are rigid bodies (the speed v encloses the mean wind speed, v_m, the rotational turbulence and the periodic components caused by tower shadow and wind share effects); v_r - relative speed of the air in relation to the blade, assuming that the tower and the

blades are flexible bodies; Ω_l and Ω_h - rotational speed to low-speed shaft and high-speed shaft, respectively; F_T - thrust force dependent of v_r, blade pitch angle, β, and tip speed ratio, $\lambda = R\Omega_l / v_r$, with R the blade length; d - tower displacement; ς - angular displacement of the blades; T_w, T_{em} - aerodynamic and electromagnetic torques. The mathematical model of this subsystem is based on thrust force, $F_T(v_r,\beta,\lambda)$ and aerodynamic torque, $T_w(v_r,\beta,\lambda)$. The expression of the thrust force, F_T, is:

$$F_T = 0.5\rho R^2 \pi C_t(\lambda,\beta)\cdot(v_r)^2 \quad (1)$$

where $C_t(\lambda,\beta)$ is the thrust coefficient dependent on λ and β, and ρ is the air density. The expression of aerodynamic torque is:

$$T_w = 0.5\rho R^3 \pi \frac{C_p(\lambda,\beta)}{\lambda}\cdot(v_r)^2 \quad (2)$$

where $C_p(\lambda,\beta)$ is the power coefficient.

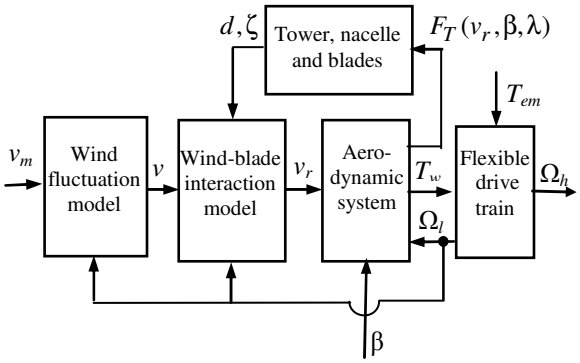

Fig. 1. The aerodynamic subsystem

The mathematical model of the tower-nacelle-blades assembly is based on the classic approach dedicated to mechanical structures with many degrees of freedom, based on the Lagrange equation [1]. The mathematical model of the drive train includes the low and high-speed shaft moving equations, as well as the elastic coupling model. The mathematical description of the tower-nacelle-blades assembly and, also, of the drive train highlight the multi-resonant character of the wind turbine.

In the model of the aerodynamic subsystem, models for damping of the tower oscillations and torsional oscillations may be optionally included.

The wind speed fluctuations in relation to wind turbine blade, $v_r(t)$, contain two components: 1) the wind speed fluctuations on the blade, $v(t)$, when the tower and the blades are considered rigid bodies and 2) the displacement of the wind turbine blade relative to the air as a result of the tower and the blades dynamics. The second component is given by the tower displacement speed, $\dot{d}(t)$, and the angular speed of the blade $\dot{\varsigma}(t)$ due to blade feathering. The equation:

$$v_r(t) = v(t) - \left(\dot{d}(t) + r_F\dot{\varsigma}(t)\right) \quad (3)$$

illustrates the two components of wind fluctuations relative to the blade, whose interaction determines the dynamics of the aerodynamic subsystem. Within the component $v(t)$, an important role is played by the rotational turbulence. There are several ways to model it: a) the solution developed by Risø National Laboratory [10] where the rotational turbulence modeling is provided by a series of second-order shaping filters which have at the input the fixed-point Kaimal turbulence; b) turbulence modeling based on superior order shaping filters [11], deduced through harmonic series methods [6], based on the fixed-point von Karman spectrum; c) turbulence modeling by simple shaping filters, in which a single concentration of power spectrum density is considered at the frequency $f_p = N_b \cdot \Omega_l / (2\pi)$, where N_b is the number of wind turbine blades [1], [12]. In this paper, the last solution was adopted. The block diagram illustrating the wind speed model with this approach is given in Figure 2. In Figures 3 a sample from the evolution of the wind speed with rotational turbulence is presented.

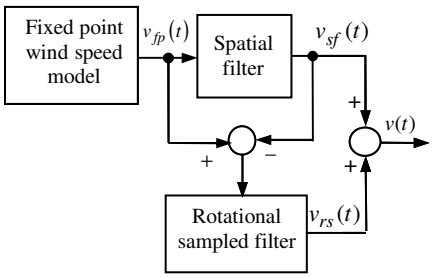

Fig. 2. Block diagram of the wind speed model

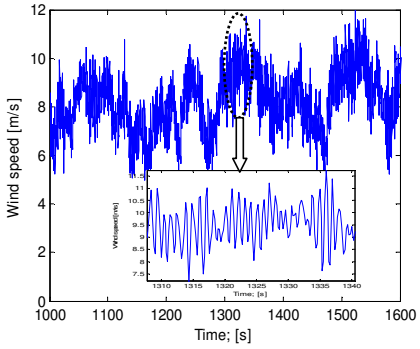

Fig. 3. Sample from the wind speed with rotational turbulence

The wind system is equipped with a squirrel cage induction generator of 2MW. The structure of the electromagnetic subsystem is given in Figure 4. The generator is vector-controlled and is enclosed in an

electromagnetic torque control loop, T_{em}, whose reference is provided by the wind system control structure. A classic model of the vector-controlled generator was used, detailed enough to include dynamic components that exceeded the bandwidth of tower oscillations, blades feathering, and torsional vibration of the drive train.

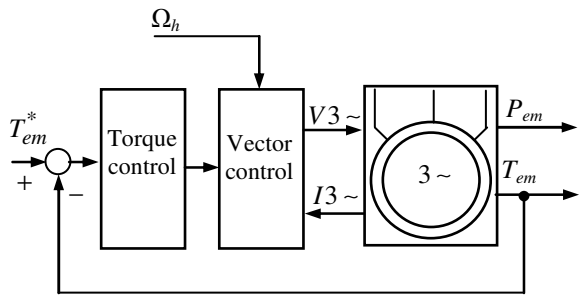

Fig. 4. The electromagnetic subsystem

B. Wind system control

The control structure of the wind system is illustrated in Figure 5. The control of the power at the demanded value in the full-load region is provided through a rotational speed control loop to high-speed shaft, Ω_h, at rated value, Ω_h^r, when in the electromagnetic subsystem it is present a stabilization loop for the electromagnetic torque to a given setpoint (rated value). In partial-load region, when the rotational speed shaft Ω_h is lower than the rated value Ω_h^r, the speed controller imposes the reference $\beta^* = 1^0$ to the blade pitch angle. The control law $T_{em}^* = F(\Omega_h)$ (Figure 5) is implemented with a lookup table bloc and encloses three operating regions: a) region 1 described by OM curve, with a parabolic shape, that ensures the wind system operation on the optimal characteristic regime; b) region 2 corresponds to the MN segment, where the rotational speed shaft Ω_h is limited (practically constant); c) regions 3 corresponds to the full-load operating region (point N), where the rotational speed shaft has the rated value, Ω_h^r. The corresponding rated value of the electromagnetic torque is $T_{em}^{*,r}$, thus resulting the rated power: $P_{em}^* = T_{em}^{*,r} \cdot \Omega_h^r = 2$ MW.

The rotational speed shaft control to the reference Ω_h^r, which further ensures the system operation in point N, is achieved by controlling the blade pitch angle. It is obvious that with shape outlined in Figure 5 the control law $T_{em}^* = F(\Omega_h)$, where the full-load operating region corresponds to point N, the system can only function satisfactorily when the wind speed has small variations, without turbulence. In the dynamic regime of the rotational speed control loop, in the presence of turbulence, the deviations of type $\Omega_h < \Omega_h^r$ determine the trajectory of the current operating point on the MN segment of the $T_{em}^* = F(\Omega_h)$ characteristic, causing a major change of the electromagnetic torque reference and, of course, of the power P_{em}. To ensure a satisfactory evolution of the power and, also, of the electromagnetic torque when the system operates in full-load region, the characteristic $T_{em}^* = F(\Omega_h)$ is chosen as in Figure 6.

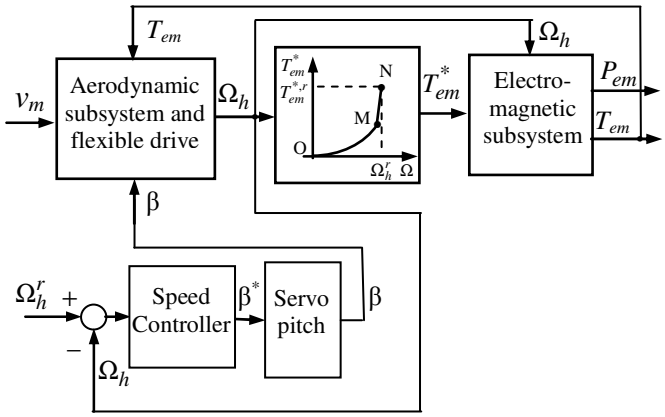

Fig. 5. The control structure

The nominal operating point in the full-load region is P, with the coordinates $\{T_{em}^{*,r}, \Omega_h^r\}$. The length of the NP segment is adopted according to the dynamic performance of the rotational speed control system and the level of rotational turbulence. The turbulence is dependent on the mean wind speed value and the site characteristics (turbulence intensity and turbulence length).

In Figure 6 the characteristic $T_{em}^* = F(\Omega_h)$ is depicted dotted when the demanded power, P_{em}^d, is adjustable. The illustration of the design procedure of the data-based controller is done for the case when the demanded power is equal to the rated one: $P_{em}^d = P_{em}^{*,r}$, and the characteristic $T_{em}^* = F(\Omega_h)$ is drawn with a full line in Figure 6.

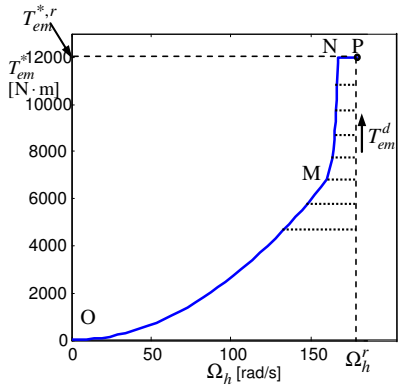

Fig. 6. The characteristic $T_{em}^* = F(\Omega_h)$

III. Data Driven Design of Rotational Speed Controller

In the full-load region, the rotational speed control loop of the high-speed shaft, Ω_h, at rated value, Ω_h^r, is made by controlling the blade pitch angle, β, in a GSC strategy. As mentioned in Section 1, the proposed data-driven controller design aims at calculating the "local" controllers within the GSC. The generic representation of a wind system variable at a given operating point is: $x(t) = \overline{x} + \Delta x(t)$, where $\overline{x}$ is the steady-state value and $\Delta x(t)$ is the deviation.

The design steps of the GSC are: 1) establishing steady state operation points in the full load region of WECS, in which the "local" controllers are computed. These steady-state operating points are defined by the pair $\{\overline{\beta}, \overline{v}_m\}$, in which $\overline{v}_m$ can be between the rated average wind speed, $v_{m,r}$, and the maximum wind speed, $v_{m,M}$, and $\overline{\beta}$ is the blade pitch angle that provides, at $\overline{v}_m$, the rotational speed Ω_h^r; 2) obtaining the input-output data record of the controlled process, $\{\Delta\beta(t), \Delta\Omega_h(t)\}$, by numerical simulation of the WECS, around the operating point for which the "local" controller is deduced; 3) computation of the "local" controllers; 4) the approximation of the characteristic of each synthesized "local" controller with the characteristic of a PI controller with the parameters K_p and T_i; 5) obtaining by interpolation of the functions $K_p(v_m)$ and $T_i(v_m)$, based on the data from the design of the "local" controllers. In this way the GSC strategy that uses a PI control law with parameters dependent on the average wind speed is obtained.

This section will present in detail the steps 3 and 4 concerning data-driven design of the local controller, considering two values of average wind speed in steady-state regime: $\overline{v}_m = 19.73$ [m/s] and $\overline{v}_m = 13.7$ [m/s].

As a starting point, it is considered an operating point corresponding to a relatively high value of the wind speed, defined by $\overline{\beta} \equiv \beta_0 = 27^0$ and $\overline{v}_m = 19.73$ m/s. The $\Delta\Omega_h(t)$ response from Figure 7 is obtained by simulating the WECS in open circuit with a random sequence of steps variation of the pitch angle $\Delta\beta(t)$. Using the records $\{\Delta\beta(t), \Delta\Omega_h(t)\}$, the data driven design procedure is based on the scheme presented in Figure 8, some of the steps being similar with the ones used in the VRFT method [13], but the method used here is essentially different. The RM block does not act as a reference model, but contributes to obtaining a reverse model of the process. The signal $\Delta\Omega_h$ is transferred by the inverse model RM^{-1}, being thus successively obtained the virtual reference $\tilde{r}$, the virtual error $\tilde{\varepsilon}$ and its integral, $\tilde{\varepsilon}_1$. Next, the data set $\{\tilde{\varepsilon}_1(t), \Delta\beta(t)\}$ is used to identify the model of the dynamic compensator (DC) so that its output signal, $\tilde{u}(t)$, "to be as close as possible" (meaning a minimum mean square error) of $\Delta\beta(t)$.

Examining the variables $\Delta y(t) = \Delta\Omega_h$ and $\tilde{\varepsilon}_1(t)$ it is found that they have very close shapes, but they are different in amplitude (Figure 9). The DC identification is made with an input signal whose shape is very close to the output of the process, $\Delta y(t)$, and with a DC output signal $\Delta u(t) = \Delta\beta(t)$, which is the input of the process. Consequently, identification will lead to a good approximation of a reverse model of the process. Under these conditions, the open-loop gain characteristic approaches that of an integrator. We can provide convenient values for the parameters of the dynamic regime (in terms of overshoot ratio and time response) by adjusting the open-loop static gain.

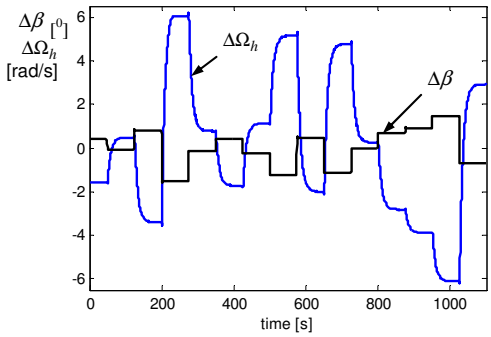

Fig. 7. The variables $\Delta\beta(t)$ and $\Delta\Omega_h(t)$ for $\overline{\beta} = 27^0$ and $\overline{v}_m = 19.73$ m/s

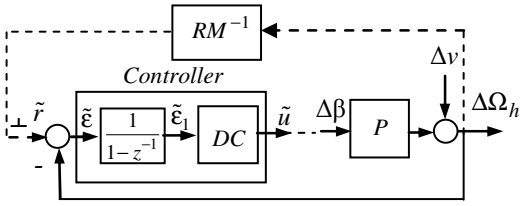

Fig. 8. The control loop structure

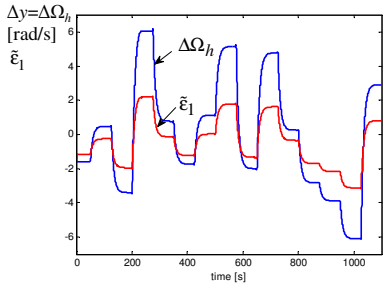

Fig. 9. The variables $\tilde{\varepsilon}_1(t)$ and $\Delta\Omega_h(t)$ for $\overline{\beta} = 27^0$ and $\overline{v}_m = 19.73$ m/s

The expressions of the reference model and the inverted model are [13], [14]:

$$H_{RM}(z^{-1}) = \frac{z^{-(n_r+1)}(1-\alpha)^{n_r}}{(1-\alpha z^{-1})^{n_r}}, \quad \alpha = \exp(-T_s\overline{\omega}) \qquad (4)$$

$$H_{RM}^{-1}(z^{-1}) = \frac{(1-\alpha z^{-1})^{n_r}}{z^{-n_r}(1-\alpha)^{n_r}} \quad (5)$$

where $n_r, \overline{\omega}$ are the parameters chosen by the designer and T_s is the sampling period. For the controller dedicated to the high mean wind speed value $\overline{v}_m = 19.73$ m/s, there have been adopted $\overline{\omega} = 1$ [rad/s] and $n_r = 2$. The DC is defined as a FIR adaptive filter with the transfer function:

$$H_{DC}(z^{-1}) = \rho \sum_{i=0}^{m} a_i z^{-i} \quad (6)$$

where the parameter ρ has initially a unitary value. The parameter m is chosen at a reduced value (e.g. $m = 2,...,4$). The dynamic compensator model can be described as follows:

$$\tilde{u}(t) = \alpha^T \varphi(t) \quad t = \overline{m, N} \quad (7)$$

with:

$$\alpha = \rho \cdot [a_0\ a_1 ... a_m]^T ; \varphi(t) = [\tilde{\varepsilon}_1(t)\ \tilde{\varepsilon}_1(t-1) ... \tilde{\varepsilon}_1(t-m)]^T \quad (8)$$

where t is the discrete time. By requiring $\tilde{u}(t)$ to optimally track $\Delta\beta(t)$ (in the sense of the mean square error), the parameters $a_i, i = \overline{1, m}$, are obtained with the RLS algorithm. For the initially imposed $m = 3$, the graphic representation of the *DC*'s Bode characteristic, given in Figure 10.

In the rotational speed control loop the presence of a very strong anti-resonance effect at high frequencies is noted. This effect is also found in the Bode characteristic of the preliminary controller (for $\rho = 1$), shown in Figure 11. The anti-resonance effect resulting in the synthesis of the dynamic compensator is the consequence of presence of the vibrations into the drive train, the main source being the torsional oscillations, plus the effect of tower oscillations and blades feathering.

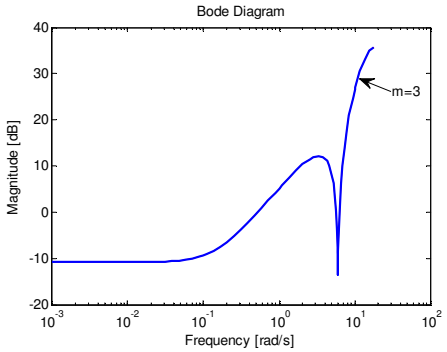

Fig. 10. The Bode characteristic of the *DC*

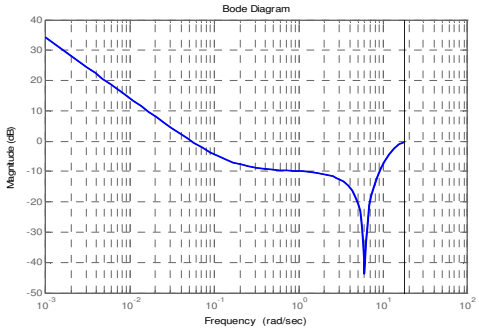

Fig. 11. The Bode characteristic of the controller (for $\rho = 1$)

As a result of the derivative character of the inverse reference model, the oscillations appear strongly amplified in the virtual reference $\tilde{r}(t)$. The oscillatory component can also be found in the virtual error $\tilde{\varepsilon}$ as well as in the variable $\tilde{\varepsilon}_1$, in the latter having a much smaller weight due to the filtering effect of the integrator. Obviously, the *DC* rejects the oscillatory component from the input through the anti-resonance effect on the frequency corresponding to these oscillations. Since this effect appears on high-frequencies and does not affect the system dynamics at low and medium frequencies, it can be neglected in the controller model. If in Figure 6 the anti-resonance effect is neglected, the Bode characteristic is very close to that of a PI controller. This result is obtained when, for the dynamic compensator synthesis, $m = 2$ is imposed. In this case the order of the *DC* is too small to include the anti-resonant subsystem and the resulting controller, with the order equal to three, has the Bode characteristic represented with solid line in Figure 12. With the Hankel analysis or the simple modal analysis, it can be reduced to a PI controller, with the Bode characteristic represented with doted line. Comparing the Bode characteristics presented in Figure 11 and Figure 12, it can be observed that the obtained PI classical controller approximates very well the Bode characteristic of the controller derived from the dynamic controller to which the anti-resonant effect is eluded.

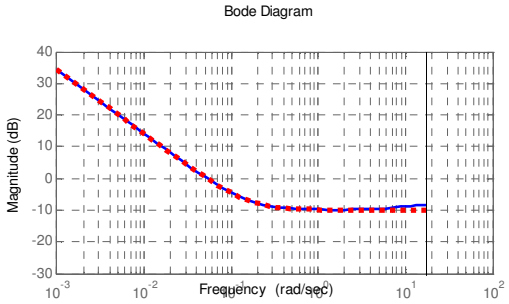

Fig. 12. Figure 12: The Bode characteristic of the synthesized controller for $m = 2$ and $\rho = 1$

The controller synthesis procedure was presented when the parameter ρ was considered for a unitary value. To determine the real value of ρ, the dataset $\{\Delta\beta(t), \Delta\Omega_h(t)\}$

is used to identify the process at the considered operating point, using the least squares of errors method.

Let be $\hat{P}(z)$ the transfer function obtained by identification. Next, the Bode plot of the open loop, with transfer function

$$H_{ol}(z)=\frac{1}{1-z^{-1}}\rho\sum_{i=0}^{m}a_i z^{-i}\cdot\hat{P}(z) \qquad (9)$$

is represented. This is practically a straight line with a slope of -20 [dB/dec] up to Shannon frequency. Then the static gain ρ is adjusted so as to reduce the duration of the dynamic regime under conditions of a stability reserve conforming to the designer's requirements.

The performance validation for the rotational speed control loop was achieved by implementing the PI controller within the wind system simulation model operating in region 3. Figure 13 presents the controlled output, Ω_h when step variations are applied to the rotational speed reference Ω_h^r. In the same graph is given the variation of the controlled output at a step variation of the mean wind speed, v_m (which is the disturbance of the closed loop system).

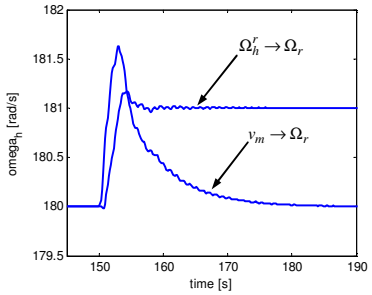

Fig. 13. The closed-loop system response $\Omega_h(t)$ for $\bar{\beta}=27^0$ and $\bar{v}_m=19.73$ m/s

Further, it has been considered an operating point located at low wind speed values that belong to the full-load operating regime of the WECS. This point is defined by $\bar{\beta}=12.7^0$ and $\bar{v}_m=13.7$ [m/s], corresponding to $\bar{\Omega}_h=$ 180 [rad/s]. From the process response obtained in this region and presented in Figure 14, it is found that the dynamic is much slower and the "non-minimum phase" effect is more pronounced. Consequently, in the *RM* bloc, $\bar{\omega}=0.5$ [1/s] was adopted, corresponding to a higher time response imposed to this block. Using a dataset $\{\Delta\beta(t),\Delta\Omega_h(t)\}$, the adopted synthesis procedure, presented above, led to a controller with similar Bode characteristic. For the reference $\Omega_h^r=180$ [rad/s], the PI controller extracted from this characteristic allows to be obtained the response from Figure 15 corresponding to the controlled output, when step variation to the reference Ω_h^r and the mean wind speed v_m have been applied.

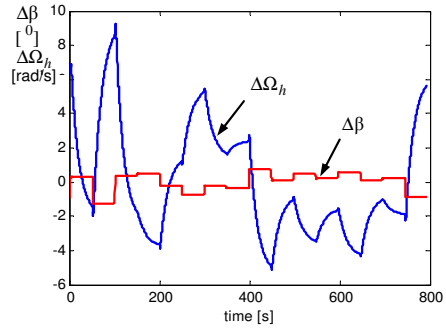

Fig. 14. $\Delta\beta(t)$ and $\Delta\Omega_h(t)$ signals for $\bar{\beta}=12.7^0$ and $\bar{v}_m=13.7$ [m/s]

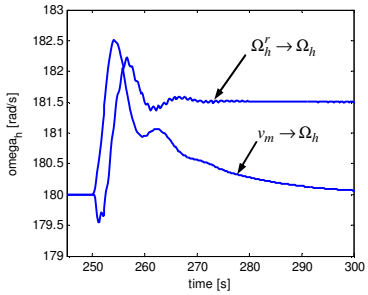

Fig. 15. The closed-loop system response $\Omega_h(t)$ for $\bar{\beta}=12.7^0$ and $\bar{v}_m=13.7$ [m/s]

Regarding the procedure for the proposed control law design, the following note should be considered:

WECS is a multi-resonant system for which two dynamic oscillatory components can be highlighted. The first component regards the wind-blade interaction, due to tower movement and blades feathering. It determines the wind speed in relation to the blade and has a crucial role in the dynamics of the entire system. The second component is the torsional oscillation, which is an important disturbing factor in the control law synthesis, because it has the most important weight in the occurrence of the anti-resonance effect in the Bode characteristic of the controller. The results above-mentioned for the controller synthesis have been obtained in the most unfavourable situation, considering that WECS is not equipped with a subsystem for torsional oscillation damping. If such a subsystem operates, a reduction of this disturbing effect is obtained. In Figure 11.a) and b) the Bode characteristics of the controller are shown, as well as the system response in a closed loop circuit to a step variation of the reference signal, when the oscillation damping subsystem is not coupled and when it is coupled, respectively.

IV. Numerical Results

Following the methodology presented in the previous section, the parameters of the PI controller have been determined for different operating points from the full-load operating regime, at which the rotational speed reference Ω_h^r is obtained, for various values of the mean wind speed,

$\overline{v}_m$. The values of the controller parameters K_p and $K_i = 1/T_i$ have been parameterized in relation with $\overline{v}_m$, thus providing a gain scheduling control.

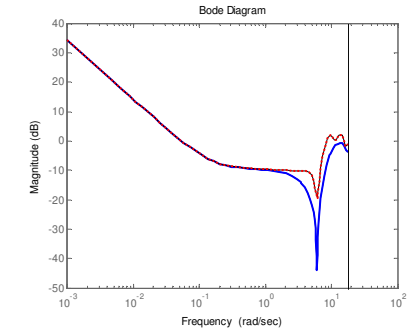

(a)

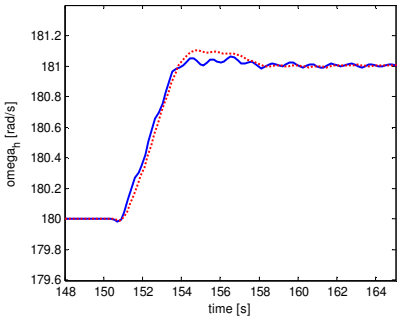

(b)

Fig. 16. The Bode characteristics (a) and the system responses (b) when torsional oscillations are damped (dot line) or not (solid line)

The next figures present the evolution of the following variables: the wind speed in relation to the blade, $v_r(t)$ (Figure 17); the high-speed shaft rotational speed $\Omega_h(t)$ (Figure 18); the electromagnetic power, $P_{em}(t)$ (Figure 19); the blade pitch angle, $\beta(t)$ (Figure 20) and the electromagnetic torque reference, $T_{em}^*(t)$ (Figure 21). The nominal wind speed for the analyzed WECS is 11.5 [m/s]. The variation in Figure 17 of wind speed causes passing twice in both directions of the WECS's regime, from partial load regime to the full load regime. By the evolutions of the mentioned variables, the control system behavior in the two operating regimes is highlighted.

The recordings in Figures 17 - 21 indicates the following:

1. The power variation in the full-load region is limited and depends on the dynamic error of the rotational speed control loop as a result of the wind speed turbulence component action. The excessive variations, caused by the movement of the current operating point on the MN region of the $T_{em}^* = F(\Omega_h)$ characteristic, are avoided. This is due to the displacement towards left of the MN region, which causes the reduction of the partial-load region where WECS power optimization is ensured;

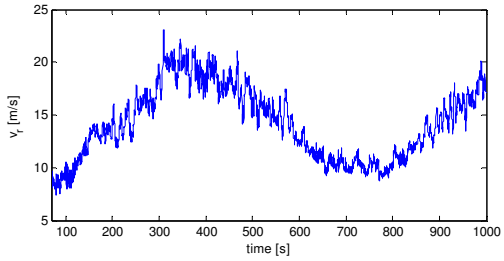

Fig. 17. The time evolution of the relative air speed $v_r(t)$

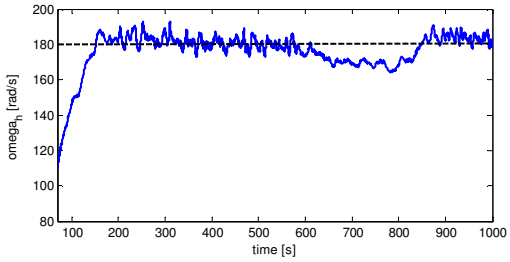

Fig. 18. The rotational speed-shaft $\Omega_h(t)$

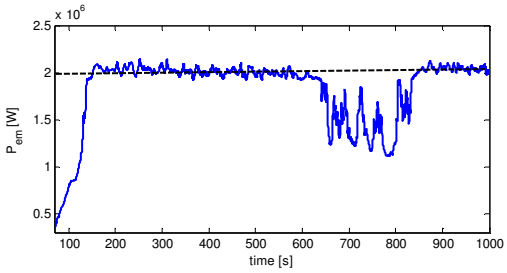

Fig. 19. The electromagnetic power $P_{em}(t)$

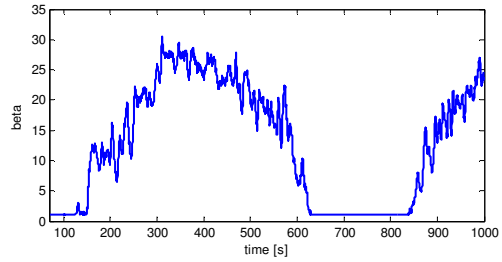

Fig. 20. The blade pitch angle $\beta(t)$

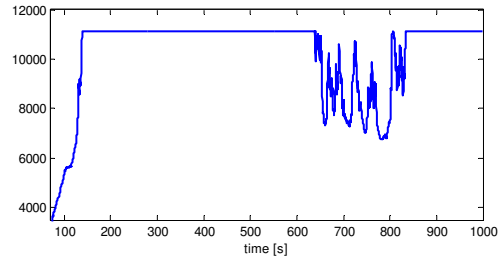

Fig. 21. The electromagnetic torque $T_{em}^*(t)$

2. In the full-load region, the generator's electromagnetic torque is kept constant, which is an important advantage for the analyzed control structure.

V. CONCLUSIONS

The proposed data-based design procedure of the controller used in this paper can quickly provide the parameters of a PI type control law for the rotational speed control loop, using data obtained by simulating detailed WECS models. The design of the "local" control laws within the gain scheduling strategy is done by selecting various operating points chosen for the regimes where the rotational speed control is performed using the blade pitch command. Given the setpoint Ω_h^r, the operating points in which the local control laws are computed are determined by: a) the demanded power $P_{em}^d = P_{em}^{*,r}$ to which it corresponds the setpoint of the electromagnetic torque $T_{em}^* = T_{em}^{*,r}$ according to the characteristic in Figure 6 and b) the average wind speed values to which the controller imposes a command $\beta(t) > \beta^* = 1^0$.

The main feature of this design procedure is the anti-resonance effect that appears in the controller's Bode characteristic. This effect has a parasitic character and is generated by the presence of torsional oscillations in the drive train. It is more or less pronounced depending on the existence/efficiency of the damping subsystem designed to alleviate these oscillations. The circumvention of this effect is justified because it occurs at high frequencies, in relation to the frequency domain that defines the essential properties of the control law.

REFERENCES

[1] F.D. Bianchi, H. De Battista, R.J. Mantz, Wind Turbine Control Systems. Principles, Modelling and Gain Scheduling Design. Springer-Verlag, 2006.

[2] C.P. Unsworth, J.E. Cater, S.E. Norris, Model predictive control of a wind turbine using short-term wind field predictions, Wind Energy, 2013,16(3), pp. 417–34.

[3] F.D. Bianchi, R.S. Sánchez-Peña, M. Guadayol, Gain scheduled control based on high fidelity local wind turbine models, Renewable Energy, 2012, 37(1), pp. 233-240

[4] A. Burlibaşa, E. Ceanga, Frequency domain design of gain scheduling control for large wind systems in full-load region, Energy Convers. and Manag., 2014, Vol. 86, pp. 204-215.

[5] F.A. Inthamoussou, H. De Battista, R.J. Mantz, LPV-based active power control of wind turbines covering the complete wind speed range, Renewable Energy, 99, 2016, pp. 996-1007.

[6] T. Burton, D. Sharpe, N. Jenkins, E. Bossanyi, Wind Energy Handbook, John Wiley&Sons, 2001.

[7] J. Jonkman, S. Butterfield, W. Musial, and G. Scott Definition of a 5-MW Reference Wind Turbine for Offshore System Development Technical Report NREL/TP-500-38060, 2009

[8] F. Iov, A.D. Hansen, P. Sørensen, F. Blaabjerg, Wind Turbine Blockset in Matlab/Simulink General Overview and Description of the Models, Aalborg University, March 2004.

[9] A.D. Hansen, F. Iov, P.E. Sørensen, N.A. Cutululis, C. Jauch, F. Blaabjerg, Dynamic wind turbine models in power system simulation tool DIgSILENT, Technical University of Denmark, Risø-R; No. 1440, 2007.

[10] P. Sørensen, A.D. Hansen, P.A. Carvalho Rosas, Wind models for simulation of power fluctuations from wind farms, Journal of Wind Engineering and Industrial Aerodynamics 2001, 90(12-15), pp. 1381-1402.

[11] A. Burlibasa, E. Ceanga, Rotationally sampled spectrum approach for simulation of wind speed turbulence in large wind turbines, Appl. Energy 2013, 111(11), pp. 624–35

[12] I. Munteanu, A.I. Bratcu, N.A. Cutululis, E. Ceangă, Optimal Control of Wind Turbine Systems. Toward a Global Approach. Springer-Verlag, 2008.

[13] M.C. Campi, A. Lecchini, S.M. Savaresi, "Virtual reference feedback tuning: A direct method for the design of feedback controllers", Automatica, vol. 38, is. 8, pp. 1337-1346, 2002

[14] M. Barbu, E. Ceanga, A data–driven approach for the design of feedback controllers, 18th Internat. Conf. on System Theory, Control and Computing – ICSTCC, Sinaia, 2014, pp. 609-614.